# Ferrocifen stealth LNCs and conventional chemotherapy: A promising combination against multidrug-resistant ovarian adenocarcinoma

Pierre Idlas, Abdallah Ladaycia, Fariba Némati, Elise Lepeltier, Pascal Pigeon, Gerard Jaouen, Didier Decaudin, Catherine Passirani

# Ferrocifen stealth LNCs and conventional chemotherapy: a promising combination against multidrug-resistant ovarian adenocarcinoma

Pierre Idlas[1], Abdallah Ladaycia[1], Fariba Némati[2], Elise Lepeltier[1*], Pascal Pigeon[3], Gerard Jaouen[3], Didier Decaudin[2,4] and Catherine Passirani[1]

[1] Micro et Nanomédecines Translationnelles, MINT, UNIV Angers, INSERM 1066, CNRS 6021, Angers, France
[2] Translational Research Department, Laboratory of preclinical Investigation, PSL University, Institut Curie, 26 rue d'Ulm, Paris 75248, France
[3] PSL Chimie Paris Tech, 11 rue P. et M. Curie and Sorbonne Université IPCM, CNRS, UMR 8232, IPCM, Paris,75005, France
[4] Department of Medical Oncology, Institut Curie, 26 rue d'Ulm, Paris 75248, France

*corresponding author

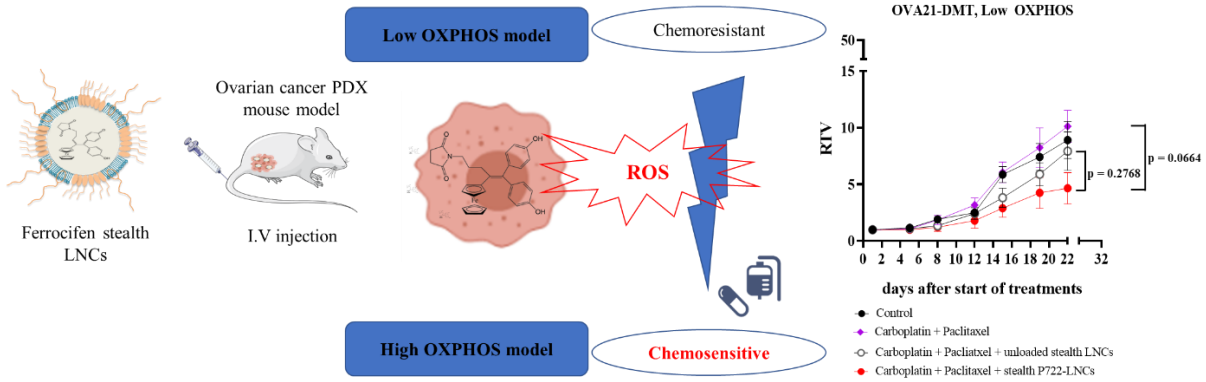


## Abstract

Ovarian cancer is one of the deadliest epithelial malignancies in women, owing to the multidrug resistance that restricts the success of conventional chemotherapy, carboplatin and paclitaxel. High grade serous ovarian carcinoma can be classified into two subtypes, the chemosensitive High OXPHOS and the Low OXPHOS tumour, less sensitive to chemotherapy. This difference of treatment efficacy could be explained by the redox status of these tumours, High OXPHOS exhibiting a chronic oxidative stress and an accumulation of reactive oxygen species. Ferrocifens, bio-organometallic compounds, are believed to be ROS producers with a good cytotoxicity on ovarian cancer cell lines. The aim of this study was to evaluate the *in vivo* efficacy of ferrocifen stealth lipid nanocapsules on High and Low OXPHOS ovarian Patient-Derived Xenograft models, alone or in combination to standard chemotherapy. Accordingly, two ferrocifens, P53 and P722, were encapsulated in stealth LNCs. The treatment by stealth P722-LNCs in combination with standard chemotherapy induced, with a concentration eight time lower than in stealth P53-LNCs, similar tumour reduction on a Low OXPHOS model, allowing us to conclude that P722 could be a leading ferrocifen to treat ovarian cancer. This combination of treatments may represent a promising synergistic approach to treat resistant ovarian adenocarcinoma.

**Keywords:** ovarian cancer, organometallic compound, multidrug resistance, Patient-Derived Xenograft model, ROS producer molecule, nanoparticle

## 1. Introduction

Ovarian cancer is the leading cause of death among gynaecological cancers. The International Agency for Research on cancer estimated that ovarian cancer could increase by 37% from 2020 to 2040 with an increase of the mortality of 48%, due especially to late diagnosis and current poor prognosis after standard chemotherapy **(1,2)**. Therefore, new treatments need to be developed. From histological analysis, three types of ovarian cancer can be characterized: stromal tumours, germ line tumours and epithelial malignancies, corresponding to 90% of ovarian cancers **(3,4)**. Among this latter histological group, around 75% of tumours are considered as High-grade serous ovarian carcinoma (HGSOC) **(3)**. They are currently treated by surgery followed by platinum-based chemotherapy and poly(ADP-ribose) polymerase (PARP) inhibitors. However, most of the patients with advanced-stage cancer develop resistance **(3–5)**. Even if cancers were first classified by histological characterization, nowadays it is well known that cancer metabolism heterogeneity is a new hallmark of tumour development **(6,7)**. Thus, Prof. Fatima Mechta-Grigoriou's team **(8)**, in using genomics, proteomics and bioenergetic analysis, showed that HGSOC could be characterized into two well-defined subtypes according to their mitochondrial metabolism: i) the High oxidative phosphorylation (High OXPHOS) tumours, which exhibit chronic oxidative stress, accumulation of reactive oxygen species (ROS) and chemosensitivity to carboplatin and paclitaxel, and ii) the Low oxidative phosphorylation (Low OXPHOS) tumours with a chemoresistance to the current treatments. This same team also highlighted the positive impact of causing oxidative stress to the Low OXPHOS tumours, as it could sensitize them to the chemotherapeutic treatment.

The use of anticancer organometallic molecules such as ferrocifens may therefore be appropriate. Indeed, since their first synthesis in the late 90s, ferrocifens, whose main series are ferrocenyl analogs of hydroxytamoxifen, ansa-ferrocenyl analogs and ferrociphenols, showed very interesting antiproliferative, cytotoxic and immunologic effects on several multi-resistance cancer cell lines **(9–11)**. The cytotoxic effect of ferrocifens was related to the unique redox properties of this organometallic family (reversible iron oxidation to the ferrocenyl moiety) leading to formation of reactive electrophile quinone methide (QM) able to interact with biological targets, and to generate ROS by a positive feedback loop **(12,13)**.

Among all the ferrocifens synthesized, the 4-ferrocenyl-5,5-bis(4-hydroxyphenyl)-pent-4-en-1-ol, designated P53, and the N-[4-ferrocenyl-5,5-bis(4-hydroxyphenyl)-pent-4-enyl]succinimide, P722, have proven to be the most efficient *in vitro* on carboplatin-resistant ovarian cancer cell lines, with $IC_{50}$ below 0.4 µM, and thus could be suitable molecules to treat the Low OXPHOS HGSOC **(14,15)** (**Figure 1.a**)).

To perform *in vivo* studies by systemic administration, the issue of the high lipophilicity of P53 and P722 (log P > 4) was overcome by using nanocarriers. In parallel to other nanocarriers such as poly(ε-caprolactone) nanocapsules or cyclodextrins, lipid nanocapsules (LNCs), a core-shell nanovector composed of an oily core and a PEGylated surfactant shell, allowed an encapsulation of these organometallic molecules with a good yield due to its oily core **(17–19)** (**Figure 1.b**)). Indeed, P53-LNCs and P722-LNCs had already been formulated and evaluated *in vivo* on multidrug resistant cancers such as glioblastoma and metastatic melanoma, confirming the choice of this nanovector and the biological efficiency of these two ferrocifen LNCs **(11,20)**. Also, in order to improve their chance of avoiding opsonization and recognition by the mononuclear phagocyte system after a systemic administration, the surface of the LNCs was shaped by adding a PEGylated phospholipid, DSPE-$PEG_{2000}$. These stealth nanocarriers have already shown an improved accumulation at the tumour site, according to the so-called Enhanced Permeation Effect (EPR effect) **(21–23)**.

However, the effectiveness of a new treatment demonstrated on animal models is too often far removed

from clinical reality and is dependent on the *in vivo* model selected. To deal with this problem, preclinical investigation can be done on well advanced, better characterized and more reproducible Patient Derived Xenograft (PDX) models, known to be more representative of the human patient tumour microenvironment and to mimic the clinical situation **(24)**. Indeed, the stability of the genomic and gene expression profiles of PDXs in mice at first transplantation and during the *in vivo* maintenance of the model, are key relevant characteristics of this approach **(25,26)**. Moreover, several studies showed that PDX models allowed a more accurate assessment of therapeutic efficiency than cell line models **(27,28)**.

The aim of this study was to evaluate the efficiency of ferrocifen stealth LNCs on High Grade and Low Grade serous ovarian cancer in mice bearing PDX, in combination or not with the current standard chemotherapy treatment of carboplatin and paclitaxel. To achieve this goal, ferrocifen-LNCs were formulated and characterized. The surface decoration by addition of a PEGylated phospholipid in order to obtain stealth nanocarriers was also performed. *In vivo* studies were first performed by systemic delivery of P53-LNCs on three High OXPHOS PDX models (OV10, OV16 and OV26) and three Low OXPHOS models (OV21, OV25 and OV54). The stealth P53-LNCs and stealth P722-LNCs were then tested on the two Low OXPHOS PDX models (OV21 and OV54), where chemotherapy was expected to be potentialized by ferrocifen-LNCs.

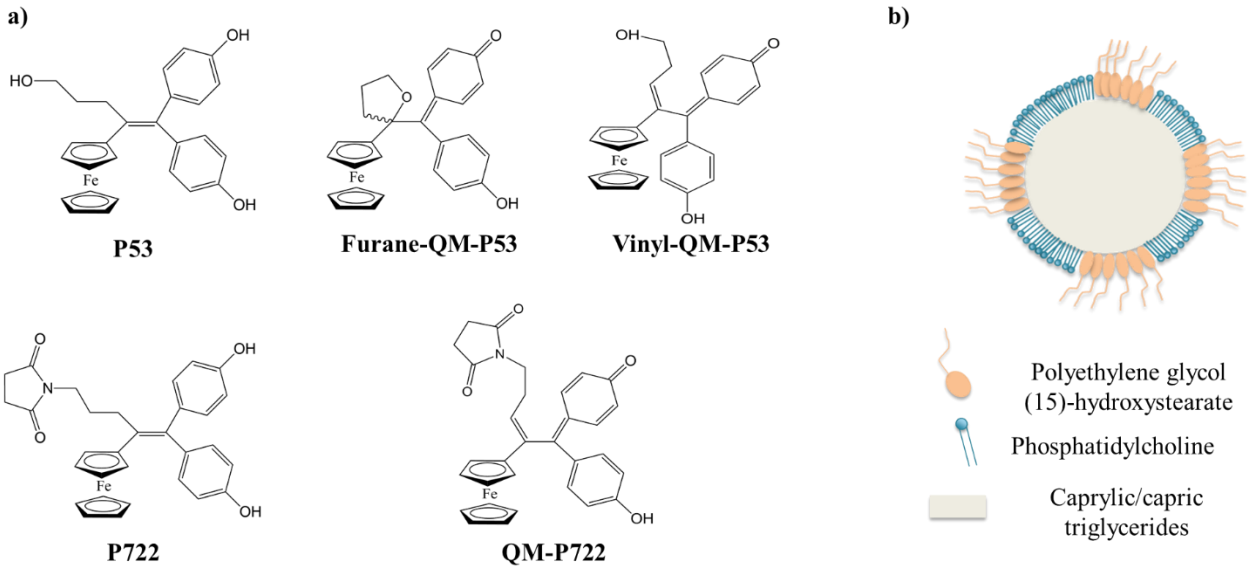


**Figure 1.** a) Molecular structures of P53 **(29)** and P722 **(15)** ferrocifens and their corresponding quinone methides (QM). Two QM can be obtained from P53 (a furane-QM-P53 and a vinyl-QM-P53); b) Schematic structure of a lipid nanocapsule (LNC).

## 2. Materials and methods

### *2.1. Chemical materials*

All components of blank LNCs, meaning non-loaded LNCs, are FDA-approved for parenteral injection. Macrogol 15 hydroxystearate (Kolliphor® HS 15) was purchased from BASF (Germany). Phosphatidylcholine from soybean (Lipoïd S 100) was provided by Lipoïd GmbH (Germany) and caprylic/capric triglycerides (Labrafac® WR 1349) were supplied by Gattefosse (France). Ultra-pure water (UPW) was obtained from a Millipore filtration system. Otherwise, all the reagents or solvents used (acetonitrile, methanol, ethanol, DMSO) for the chromatography analysis were of analytical grade. P53 and P722 ferrocifens were synthesized and provided by PSL Chimie ParisTech (France) according

to Pigeon *et al.* **(15,29)**. 1,2-distearoyl-*sn*-glycero-3-phosphoethanolamine-N-[methoxy(polyethylene glycol)-2000] (DSPE-mPEG$_{2000}$) (Mean Molecular Weight (MMW) = 2805 g/mol) was purchased from Avanti Polar Lipids (Alabaster, USA).

### *2.2. Preparation of blank LNCs*

Blank LNCs were prepared by a phase inversion process as comprehensively described in the literature **(30)**. Firstly, all the excipients, Kolliphor® HS 15 (16.9 % w/w), Lipoïd S 100 (1.5 % w/w), Labrafac® WR 1349 (20.7 % w/w), NaCl (1.3 % w/w, with respect to physiological osmolarity) and UPW (59.6 % w/w) were mixed under magnetic stirring at 60 °C for 10 min. Three heating-cooling cycles were performed between 90 °C and 60 °C to obtain the emulsion phase inversion (O/W emulsion for temperature lower than phase inversion temperature (PIT) and W/O emulsion for temperature higher than PIT). During the third cycles, when the temperature decreased and reached the PIT (78 °C < PIT < 83 °C), ice-cold UPW (31.5 % v/v$_{tot}$) was added to induce an irreversible shock and to finally obtain the LNCs. The suspension was then stirred for 10 min under slow magnetic stirring at room temperature. To finish, the LNC formulation was filtrated through 0.2 µm sterile polyethersulfone (PES) membrane to remove any aggregates and to sterilize for intravenous injection before storage at 4 °C.

### *2.3. Preparation of P53-LNCs*

In order to formulate P53-LNC, ethanol was used (0.01% V/V$_{tot}$) in order to improve the dispersion of P53 (powder form) in Labrafac. The solvent was then evaporated via argon flow, followed by addition of the other excipients. The same phase inversion process was then performed, and finally the P53-LNC formulation was filtrated through 0.2 µm sterile PES membrane and stored at 4 °C.

### *2.4. Preparation of P722-LNCs*

In order to formulate P722-LNC, P722 (powder form) was added with Kolliphor® HS 15 and Labrafac® WR 1349 and stirred for 30 min at 60 °C. Then the other excipients (Lipoïd S 100, NaCl and UPW) were added and the three heating-cooling cycles of the phase inversion process were applied. The obtained P722-LNCs were filtrated through 0.2 µm sterile PES membrane and stored at 4 °C.

### *2.5. Post-insertion by DSPE-PEG$_{2000}$*

The PEGylated phospholipid used was the 1,2-distearoyl-*sn*-glycero-3-phosphoethanolamine-N-[methoxy(polyethylene glycol)-2000] (DSPE-mPEG$_{2000}$). To obtain stealth LNCs, this polymer was post-inserted at the LNC surface at the concentration of 5 mM, as previously described **(31)**. Briefly, the DSPE-mPEG$_{2000}$ (powder form) was added to blank LNCs, P53-LNCs or P722-LNCs, put under magnetic stirring at 30 °C for 4 h and then quenched for 1 min in an ice bath. All stealth formulations were then filtrated through sterile PES membrane and stored at 4 °C.

### *2.6. Characterization of the lipid nanocapsules*

Average hydrodynamic diameter and polydispersity index (PDI) were determined by the dynamic light scattering technique at 25 °C with a backscatter angle of 173 ° using a Zetasizer Nano ZS system (Malvern Instrument Ltd, UK) after optimum dilution of the formulations in UPW. The measured average values were calculated from 3 runs, with more than 10 measurements for each run.

Zeta potential of the nano-systems was measured using the laser Doppler micro-electrophoresis technique by a Zetasizer Nano ZS system (Malvern Instrument LtD, UK). The measured average values were calculated from 3 runs with more than 10 measurements for each run, after a dilution by 100 of the formulations with UPW (pH = 8.3 at 25°C). Smoluchowski's approximation was used to determine electrophoretic mobility for determination of the zeta potential. For size, PDI and zeta potential, results

shown in **Table 1** are the average of at least three formulations (n > 3).
Drug loading and encapsulation efficiency (E.E) for each ferrocifen (P53 and P722) were determined using Ultra-High-performance liquid chromatography (UPLC) methods. A C18 analytical column (Waters, France) was used at 20 °C. For each molecule, the quantification of encapsulated ferrocifens was obtained by a UV detector at λ = 450 nm, after the filtration step on 0.2 µm and a dissolution of LNCs with the optimal solvent described below. Analysis of the data was performed using Empower 3 software (Waters).
For P53-LNCs, C18 column was eluted at a flow rate to 0.2 $mL.min^{-1}$ with ethanol and water (80/20 v/v). Calibration curves were established (at each analysis) by quantifying the area under the curves (AUCs) of [0.4 – 2] $mg.mL^{-1}$ P53 solutions in ethanol. The LNCs were dissolved by a 10-fold dilution in ethanol and quantification of the P53 was performed using the calibration curve. Injection volume was 2 µL and retention time of P53 was 0.7 min.
For P722-LNCs, C18 column was eluted at a flow rate to 0.2 $mL.min^{-1}$ with acetonitrile and water (65/35 v/v). Calibration curves were established (at each analysis) by quantifying the area under the curves (AUCs) of [0.025 – 0.125] $mg.mL^{-1}$ P722 solutions in blank LNCs dissolved by a 40-fold dilution in methanol/DMSO (90/10 v/v). The LNCs were broken by a 40-fold dilution with methanol/DMSO (90/10 v/v) and the quantification of the P722 was performed using the calibration curve. Injection volume was 5 µL and retention time of P722 was 1.2 min.

Encapsulation efficiency (E.E, %) of the corresponding ferrocifen in LNCs was calculated using the following equation:

$$E.E\ (\%) = \frac{(Total\ ferrocifen\ conc.in\ LNC - unencapsulated\ ferrocifen\ conc.in\ LNC)}{Initial\ drug\ conc.\ in\ LNC} \times 100$$

Drug loading of the corresponding ferrocifen in LNCs was calculated using the following equation:

$$D.L\ (\%\ w/w) = \frac{Mass\ of\ encapsulated\ ferrocifen\ in\ 1\ mL\ of\ LNC\ dispersion}{m(ferrocifen) + m(Labrafac®\ WR\ 1349\ ) + m(Kolliphor®\ HS\ 15\ ) + m(Lipoïd\ S\ 100)} \times 100$$

### *2.7. In vivo study on Patient-Derived Xenograft Models*

PDX models of High Grade serous ovarian carcinoma tumours were established at the Institut Curie (Paris, France) with patient consent, according to the relevant national law on the protection of participants in biomedical research.
Briefly, tumour fragments from patients were grafted into the interscapular fat pad, a highly vascularized area, of 6-week-old-female Swiss nude mice under avertin anaesthesia. After two to twelve months of development, the tumours were retained and cut into three new fragments in order to be grafted again in three nude mice. This step was repeated three time to reach tumour stability.
Six models derived from six different patients were selected: three High OXPHOS models (OV10, OV16 and OV26) and three Low OXPHOS models (OV21, OV25 and OV54). The genomic analysis, homologous repair deficiency (HRD) – homologous repair proficiency (HRP) status and the mitochondrial metabolism of the six models were well described in the literature **(8,32)**. The protocol for the treatment of mice was adapted over time according to the results obtained with the first formulation tested, P53-LNCs.
In all experiments, LNCs, P53-LNCs or P722-LNCs were injected intravenously at 5 mL/kg of mice, twice per week, by tail-vein or retro-orbital injections. Conventional chemotherapies, carboplatin and paclitaxel, were administered intraperitoneally at 10 mL/kg, every 2 weeks for the preliminary study and

every 3 weeks for the second part of the study. The control groups were treated intravenously with NaCl 0.9 %.

- *Preliminary study*

As a preliminary study, a formulation of P53-LNCs at a drug loading of 2.73 % (w/w) was first evaluated on the three High OXPHOS models (OV10, OV16 and OV26) and the three Low OXPHOS models (OV21, OV25 and OV54). Mice were divided into eight random groups in accordance with the eight different treatments or combination of treatments to be tested ($3 \leq n \leq 5$ mice per group). Administration of conventional chemotherapy was performed at a dose of 66 mg/kg for carboplatin and a dose of 30 mg/kg for paclitaxel. Blank and P53-LNCs at 2.73 % (w/w) were injected at full dose (38 mg of P53/kg) and half dose (19 mg of P53/kg, obtained by dilution). Blank and P53-LNCs were administered alone or in combination with the conventional chemotherapy for the study. Details of the protocol of treatment are summarized in **Table 2**.

- *Second part of the study*

For the second part of the study, two PDX models were selected, according to the results obtained above: the Low OXPHOS models OV21 and the OV54.
Stealth P53-LNCs at a maximum drug loading of 4.36 % (w/w) were evaluated. The mice were divided in ten random groups in accordance with the ten different treatments or combination of treatments to be tested ($5 \leq n \leq 8$ mice per group). Administration of conventional chemotherapy was performed at half dose for both chemotherapy, carboplatin (33 mg/kg) and paclitaxel (15 mg/kg) in order to highlight the potential effect of the ferrocifen suspensions. The stealth blank and P53-LNCs at 4.36 % (w/w) were injected at full dose (65 mg of P53/kg) and half dose (32.5 mg of P53/kg mouse, obtained by dilution), alone or in combination with the conventional chemotherapy. Details of the treatment protocol are summarized in **Table 3**.
Stealth P722-LNCs at a maximum drug loading of 0.56 % (w/w) were then evaluated. The mice were divided in six random groups in accordance with the different treatments or combination of treatments to be tested ($5 \leq n \leq 7$ mice per group). Administration of conventional chemotherapy was performed at half dose for both carboplatin (33 mg/kg) and paclitaxel (15 mg/kg). The stealth blank and P722-LNCs at 0.56 % (w/w) were injected at a dose of 8 mg of P722/kg, alone or in combination with the conventional chemotherapy. Details of the treatment protocol are summarized in **Table 4**.
Mice bearing tumours with a volume from 50 to 150 $mm^3$ were individually identified and randomly assigned to the control or treatment groups. Tumour growth was assessed twice a week by measuring two perpendicular diameters of tumours using a calliper. Individual mouse tumour volume was calculated as follows, $V = a \times b^2/2$, with $a$ the major diameter and $b$ the minor diameter. The tumour volume evolution at day n ($V_n$) was expressed as relative tumour volume (RTV) according to the following formula: $RTV = V_n/V_0$ with $V_0$ being the initial volume at time of inclusion.
Antitumour activity was evaluated according to tumour growth inhibition (TGI), calculated according to the following formula: $TGI\% = 100 - (RTVt/RTVc \times 100)$, where *RTVt* is the median *RTV* of treated mice and *RTVc* is the median *RTV* of controls, both at a given time point when the antitumour effect was optimal. A meaningful biological effect was defined as a TGI of at least 50%. Statistical significance of differences observed between the individual *RTV* corresponding to the treated mice and control groups was calculated by the two-tailed Mann-Whitney test. Growth delay index was calculated as the time required to reach the same RTV in the treated and control groups, at a RTV of 2.
Moreover, an overall response rate (ORR) was calculated for each treated mouse as follows: [(*RTVt/mRTVc*)], where *RTVt* is the relative tumour volume of the treated mouse and *mRTVc* is the median relative tumour volume of the corresponding control group at the end of treatment. [(RTVV)-1] for each

treated mouse was then calculated: a tumour was considered to be responding to treatment if [(RTVV)-1] was below -0.5.
All *in vivo* experimental procedures were specifically approved by the ethics committee of the Institut Curie CEEA-IC #118 (Authorization APAFiS# 25870-2020060410487032-v1 given by National Authority) in compliance with the international guidelines.

## 3. Results and Discussion

### *3.1. Physico-chemical properties of LNC suspensions*

**Table 1:** Physico-chemical characteristics (size, PDI, zeta potential, drug loading and encapsulation efficiency) of blank LNCs, stealth LNCs with or without P53 and P722.

| Formulation | Hydrodynamic diameter (nm) | PDI | Zeta Potential (mV) | Drug loading (% w/w) | Encapsulation efficiency (E.E) (%) |
|---|---|---|---|---|---|
| Blank LNCs | 53.6 ± 1.0 | 0.05 ± 0.01 | -2.7 ± 1.3 | - | - |
| Stealth blank LNCs | 60.7 ± 2.3 | 0.06 ± 0.01 | -18.3 ± 1.8 | - | - |
| P53-LNCs | 46.0 ± 0.8 | 0.05 ± 0.01 | -1.8 ± 0.1 | 2.73 | > 97 % |
| Stealth P53-LNCs | 49.1 ± 0.2 | 0.10 ± 0.01 | -20.8 ± 0.1 | 4.36 | > 96 % |
| P722-LNCs | 50.9 ± 0.2 | 0.06 ± 0.01 | -1.7 ± 0.8 | 0.56 | > 95 % |
| Stealth P722-LNCs | 57.2 ± 1.0 | 0.06 ± 0.01 | -18.1 ± 0.4 | 0.56 | > 95 % |

LNCs were prepared by a phase-inversion process as previously described **(30)**. The different ferrocifens (P53 and P722) were added at the beginning of the process. The P53 drug loading was set first at 2.73 % (w/w) for conventional LNCs and reaching its maximal value at 4.36 % (w/w) for stealth LNCs with an encapsulation efficiency (E.E) higher than 95 % for both formulations. For the P722, the maximal drug loading was 0.56 % (w/w) with an E.E also higher than 95 %. The difference in drug loading between these ferrocifens may be explained by the lipophilicity of the molecules as reported in the literature. Indeed, P53 has a logPo/w higher than P722 (4.2 and 4.0 respectively) **(15)**, meaning that P53 is 1.6 times more lipophilic than P722. It might also be correlated to the 3D structure of P722 in which the phenol in trans position to ferrocene would be less lipophilic than the trans-one in P53. By analogy to the quinone methide from P722, the succinimide from P722 could modify the electronic environment of the phenol due to the π-stacking and so modify the lipophilicity of the hydroxyl group **(33)**.

LNC hydrodynamic diameters, polydispersity indexes (PDI) and zeta potentials are given in **Table 1**. Whichever the ferrocifen used and whatever the initial amount added, monodispersed formulations were obtained: PDIs ≤0.1. Blank LNCs, P53-LNCs and P722-LNCs had a hydrodynamic diameter of 53.6 ± 1.0 nm, 46.0 ± 0.8 nm and 50.9 ± 0.2 nm with a zeta potential of -2.7 ± 1.3 mV, -1.8 ± 0.1 mV and -1.7 ± 0.8 mV respectively, close to neutrality. After the post-insertion of the PEGylated phospholipid DPSE-$PEG_{2000}$ at a concentration of 5 mM, a slight increase of the diameters was observed (variation between 6 % and 12 % according to the formulations), followed by a clear decrease of the zeta potential (values lower than -18.0 mV). This classical decrease of the zeta potential after surface decoration by a PEG shell is explained by the electrical dipole of the PEG moiety **(34)**.

The formulations of the P53 and P722 ferrocifens were thus successful and in accordance with the previous studies performed in the same research laboratory **(11,20)**.

*3.2. Preliminary in vivo studies of P53-LNCs on the different PDX models*

In order to test the efficacy of the formulated P53-LNCs in ovarian cancer, three high OXPHOS PDX models (OV10, 0V16 and OV26) and three low OXPHOS PDX model (OV21, OV25 and OV54) were treated. Different groups were formed: a control group treated with saline solution (NaCl 0.9 %), and groups treated with different concentrations of blank LNCs, P53-LNCs, chemotherapy, and combination of chemotherapy with P53-LNCs at full dose and half dose (**Table 2**).

**Table 2:** Summary of the different groups treated by P53-LNCs at 2.73 % (w/w) alone or in combination with conventional chemotherapy (carboplatin and paclitaxel). Carboplatin and paclitaxel were intraperitoneally injected once every two weeks at full dose (66 mg/kg and 30 mg/kg respectively). Blank or P53-LNCs were intravenously administered twice per week at full dose FD (38 mg/kg) or half dose HD (19 mg/kg).

| Treatment | Composition | Dose of anticancer drug (mg/kg) |
|---|---|---|
| **Control** | NaCl 0.9 % | - |
| **B-LNCs** | Full dose, blank LNCs | eq. 38* |
| **FD P53-LNCs** | Full dose, P53-LNCs | 38 |
| **HD P53-LNCs** | Half dose (by dilution), P53-LNCs | 19 |
| **CPt + TAX** | Carboplatin + paclitaxel | 66 + 30 |
| **B-LNCs + CPt + TAX** | Blank LNCs + carboplatin + paclitaxel | eq. 38* + 66 + 30 |
| **FD P53-LNCs + CPt + TAX** | Full dose P53-LNCs + carboplatin + paclitaxel | 38 + 66 + 30 |
| **HD P53-LNCs + CPt + TAX** | Half dose P53-LNCs + carboplatin + paclitaxel | 19 + 66 +30 |

eq. 38* indicates that the same concentration in excipients than the full dose P53-LNCs was administered.

First, tolerance to the treatments was evaluated. The results obtained showed the absence of a significant weight loss of the treated groups, indicating a good tolerance of the different treatments by the mice (**Figure S2**. in supplementary information).

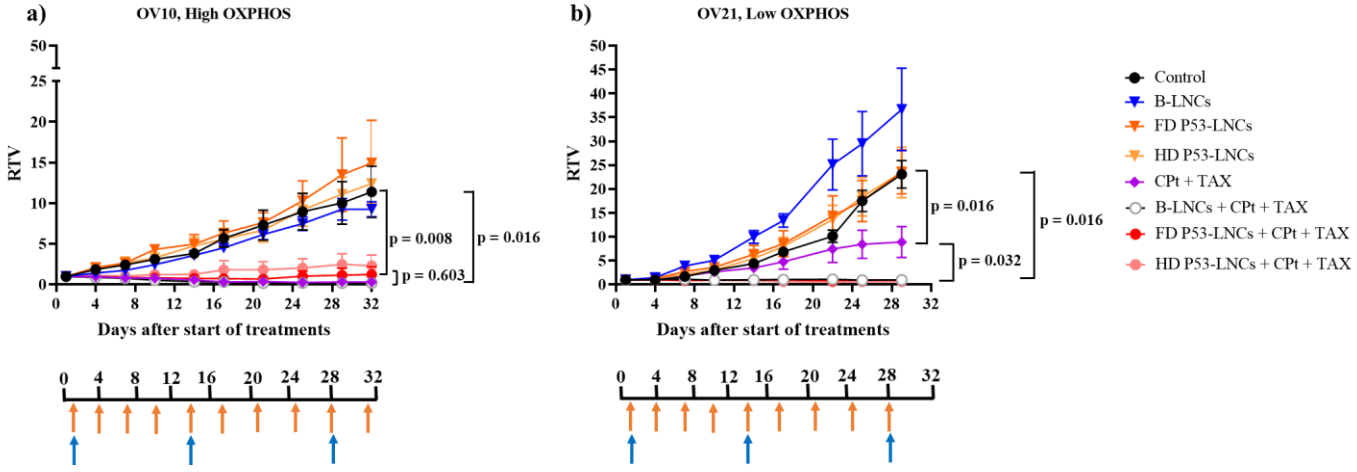


**Figure 2.** Tumour growth curves (relative tumour volumes *[RTV]* = $V_n/V_0$ as a function of time) of: a) High OXPHOS model OV10 and b) Low OXPHOS model OV21 after different treatments, summarized in **Table 2**. Timelines indicated days of treatment injection for P53-LNCs or blank LNCs (orange arrow) and for chemotherapies (blue arrow). Data are means ± SEM ($3 \leq n \leq 5$ mice per group). Statistical analysis was performed with a Mann-Whitney test to compare two groups each other. Data were considered significant for $p < 0.05$.

The chemotherapy treatment, applied on three High OXPHOS (OV10, OV16 and OV26) and three Low OXPHOS (OV21, OV25 and OV54) ovarian cancer models, showed a better response on the High OXPHOS models confirming the results of Mechta Gregouriou *et al.* **(8)** (**Figure 2.a** and **Figure S3** in

supplementary information). Indeed, on the last day of measurement (last day where all animals are alive in all groups), chemotherapy "CPt + TAX" (**Table 2**) led to a significant tumour growth inhibition (TGI) of above 90 % compared to NaCl 0.9 % "control" (**Table 2**) whatever the High OXPHOS model used, whereas on the Low OXPHOS models OV21 and OV25, a TGI of only 61 %, still significant was obtained with chemotherapy "CPt + TAX" compared to NaCl 0.9 % (**Figure 2.b** and **Figure S3**. in supplementary information). Moreover, whatever the model used, Full Dose P53-LNCs "FD P53-LNCs" and Half Dose P53-LNCs "HD P53-LNCs" (**Table 2**) did not impact the tumour growth compared to chemotherapy "CPt + TAX". Hence, it was hypothesized that the majority of P53-LNCs could not reach the tumour site due to rapid recognition by the mononuclear phagocyte system. Indeed, even if the surface of the LNCs is composed of PEG moieties, the steric hindrance from these short chains of PEG (15 PEG monomer units) might not be efficient to avoid the opsonization phenomenon. That is why, for the rest of the project, the formulations were modified by adding a longer PEGylated phospholipid, with 45 PEG monomer units, in order to confer stealth properties to the formulation **(20, 31)**.

Furthermore, no difference was obtained between standard chemotherapy "CPt + TAX" and in combination with P53-LNCs "FD P53-LNCs + CPt + TAX" (**Table 2**) on the three High OXPHOS and two Low OXPHOS models (OV54 and OV25) (**Figure 2** and **Figure S3.** in supplementary information). For the Low OXPHOS model OV21, a significant decrease in RTV of 90 % was observed between "FD P53-LNCs + CPt + TAX" and "CPt + TAX". However, the same biological response is observed with the treatment "B-LNCs + CPt +TAX".

Thus, for further studies, the dose of carboplatin and paclitaxel was reduced by half with intraperitoneal injection once every three weeks instead of once every two weeks and the P53 payload in LNCs increased to 4.36 % (the highest possible) in order to highlight the biological effect of the ferrocifen-LNCs. Finally, only the low OXPHOS model OV21 and OV54 were used for further experiments, as they were the most resistant to chemotherapy.

### *3.3. In vivo activity of stealth P53-LNCs on the selected PDX models*

**Table 3:** Summary of the different groups of treatment by stealth P53-LNCs at 4.36 % (w/w) alone or in combination with conventional chemotherapy (carboplatin and paclitaxel). Carboplatin and paclitaxel were intraperitoneally injected once every three weeks at half dose (33 mg/kg and 15 mg/kg respectively). Stealth blank LNCs and stealth P53-LNCs were intravenously administered twice per week at full dose FD (65 mg/kg) and half dose HD (32.5 mg/kg).

| Treatment | Composition | Dose of anticancer drug (mg/kg) |
|---|---|---|
| **Control** | Control (NaCl 0.9 %) | - |
| **FD S-B-LNCs** | Full dose, stealth blank LNCs | eq. 65* |
| **HD S-B-LNCs** | Half dose, stealth blank LNCs | eq. 32.5 |
| **FD P53-S-LNCs** | Full dose, stealth P53-LNCs | 65 |
| **HD P53-S-LNCs** | Half dose, stealth P53-LNCs | 32.5 |
| **CPt + TAX** | Half dose, Carboplatin + paclitaxel | 33 + 15 |
| **FD S-B-LNCs + CPt + TAX** | Full dose, stealth blank LNCs + carboplatin + paclitaxel | eq. 65 + 33 + 15 |
| **HD S-B-LNCs + CPt + TAX** | Half dose, stealth blank LNCs + carboplatin + paclitaxel | eq. 32.5 + 33 + 15 |
| **FD P53-S-LNCs + CPt + TAX** | Full dose, stealth P53-LNCs + carboplatin + paclitaxel | eq. 65 + 33 + 15 |
| **HD P53-S-LNCs + CPt + TAX** | Half dose, stealth P53-LNCs + carboplatin + paclitaxel | eq. 32.5 + 33 +15 |

eq. 65* indicates that the same concentration in excipients than the full dose stealth P53-LNCs was administered

In order to test the efficacy of the formulated stealth P53-LNCs in ovarian cancer, two PDX models of the Low OXPHOS subtypes of ovarian cancer (OV21 and OV54) were chosen. Different groups were

formed: a control group treated with saline solution (NaCl 0.9 %), and groups treated with different concentrations of blank LNCs, stealth P53-LNCs, chemotherapy, and combination of chemotherapy with stealth P53-LNCs at full dose and half dose (**Table 3**).

First, tolerance studies were performed. As in the preliminary experiment with P53-LNCs, the absence of a significant weight loss of the treated groups was observed, indicating a good tolerance of the different treatments by the mice (**Figure S4.a** in supplementary information).

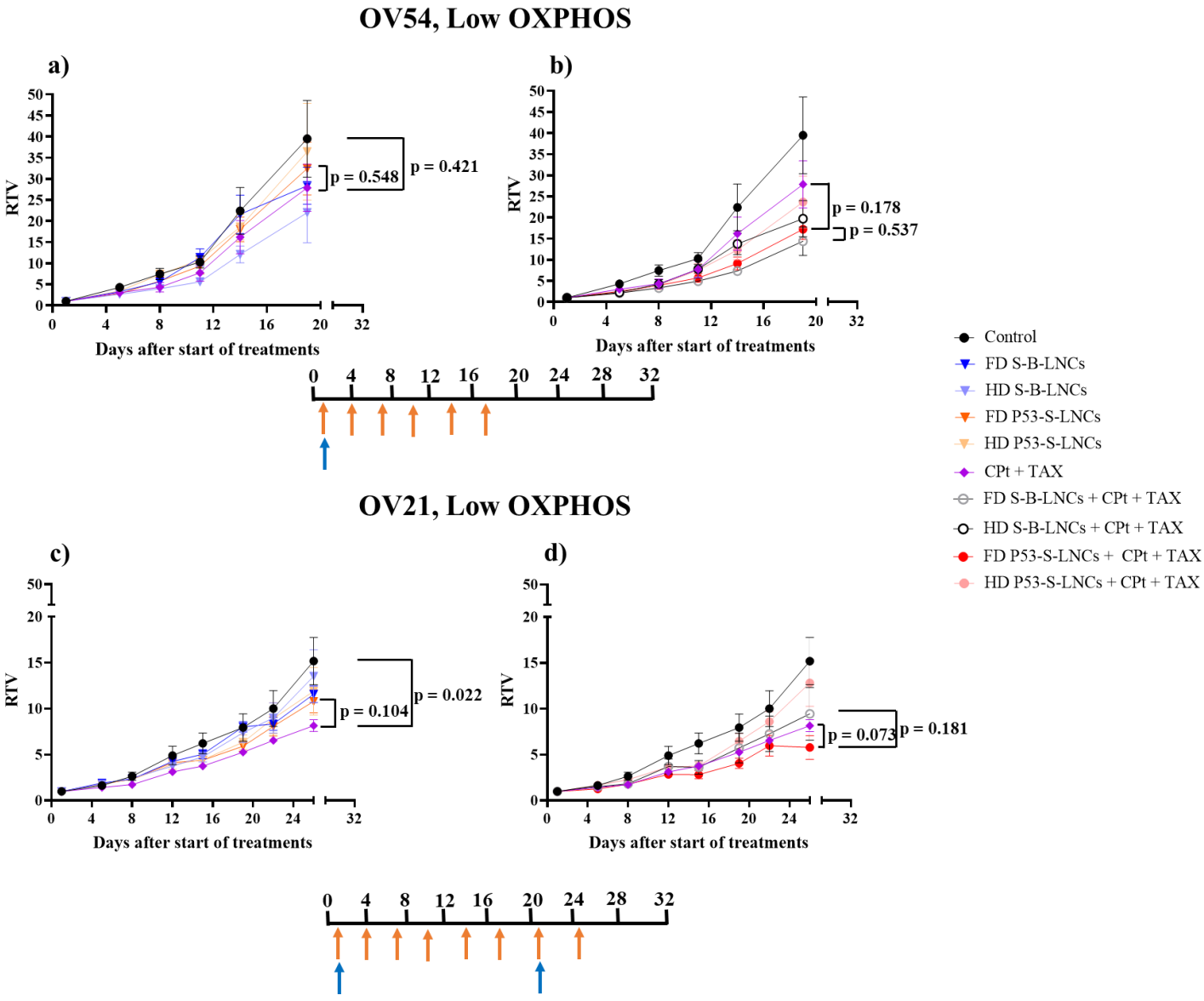


**Figure 3.** a) Comparison of the RTV as a function of time of the Low OXPHOS model OV54 treated by stealth blank LNCs "FD S-B-LNCs" (blue triangle), stealth P53-LNCs "FD P53-S-LNCs" (orange triangle) and chemotherapy "CPt + TAX" (purple diamond) ; b) Comparison of the RTV as a function of time of the Low OXPHOS model OV54 treated with the combination of stealth blank LNCs and chemotherapy "FD S-B-LNCs + CPt + TAX" (empty grey circle), combination of stealth P53-LNCs and chemotherapy "FD P53-S-LNCs + CPt + TAX" (red circle) and chemotherapy "CPt + TAX" (purple diamond) ; c) Comparison of the RTV as a function of time of the Low OXPHOS model OV21 treated with stealth blank LNCs "FD S-B-LNCs" (blue triangle), stealth P53-LNCs "FD P53-S-LNCs" (orange triangle) and chemotherapy "CPt + TAX" (purple diamond) ; d) Comparison of the RTV as a function of time of the Low OXPHOS model OV21 treated with the combination of stealth blank LNCs and chemotherapy "FD S-B-LNCs + CPt + TAX" (empty grey circle), combination of stealth P53-LNCs and chemotherapy "FD P53-S-LNCs + CPt + TAX" (red circle) and chemotherapy "CPt + TAX" (purple diamond). Timelines indicated days of treatment injection for P53-LNCs or blank LNCs (orange arrow)

and for chemotherapies (blue arrow). Data are means ± SEM ($5 \leq n \leq 8$ mice per group). Statistical analysis was performed with a Mann-Whitney test to compare two groups each other. Data were considered significant for $p < 0.05$.

**Table 4:** Relative tumour volume ([RTV] = $V_n/V_0$, n corresponding to the end of experiment) and tumour growth inhibition ([TGI] = $100 - (RTVt/\ RTVc \times 100)$) after different treatments, summarized in Table 3, on the two Low OXPHOS model OV21 and OV54.

| | **Treatment** | **RTV (%) (day 19)** | **TGI (%) (day 19)** |
|---|---|---|---|
| **OV54** | Control | 39.5 | 0.0 |
| | FD S-B-LNCs | 28.4 | 28.2 |
| | HD S-B-LNCs | 22.0 | 44.3 |
| | FD P53-S-LNCs | 32.5 | 17.9 |
| | HD P53-S-LNCs | 36.4 | 7.8 |
| | CPt + TAX | 27.9 | 29.4 |
| | FD S-B-LNCs + CPt + TAX | 14.4 | 63.5 |
| | HD S-B-LNCs + CPt + TAX | 19.8 | 50.0 |
| | FD P53-S-LNCs + CPt + TAX | 17.2 | 56.4 |
| | HD P53-S-LNCs + CPt + TAX | 23.7 | 40.0 |
| | | **RTV (%) (day 26)** | **TGI (%) (day 26)** |
| **0V21** | Control | 15.2 | 0.0 |
| | FD S-B-LNCs | 11.6 | 23.7 |
| | HD S-B-LNCs | 13.6 | 10.8 |
| | FD P53-S-LNCs | 10.8 | 28.9 |
| | HD P53-S-LNCs | 11.9 | 21.6 |
| | CPt + TAX | 8.2 | 46.3 |
| | FD S-B-LNCs + CPt + TAX | 9.5 | 37.8 |
| | HD S-B-LNCs + CPt + TAX | 10.1 | 33.5 |
| | FD P53-S-LNCs + CPt + TAX | 5.8 | 61.9 |
| | HD P53-S-LNCs + CPt + TAX | 12.8 | 15.6 |

On the Low OXPHOS model OV54, the stealth P53-LNCs at full dose or half dose ("FD P53-S-LNCs" and "HD P53-S-LNCs") and chemotherapy "CPt + TAX" did not impact the tumour growth compared to NaCl 0.9 % "control", with a TGI of 17.9 %, 7.8 % and 29.4 % respectively (**Figure 3.a and Table 4**). When combining stealth P53-LNCs with carboplatin and paclitaxel "FD P53-S-LNCs + CPt + TAX", a TGI of 56.4 % was obtained but it was not possible to conclude if this efficiency was due to P53 as a TGI of 63.54 % was obtained with combination of stealth blank LNCs and chemotherapy "FD S-B-LNCs + CPt + TAX" (**Figure 3.b and Table 4**). These results underline the fact that the excipients of the LNC itself can produce a biological response: indeed, due to their lipid nature, blank LNCs could enhance the internalization of carboplatin and paclitaxel in the cell cytoplasm by destabilizing the cell membrane. This potential adjuvant effect of blank LNCs will be tested in further studies.

On the Low OXPHOS model OV21, the stealth P53-LNCs at full dose or half dose ("FD P53-S-LNCs" and "HD P53-S-LNCs") did not improve the biological response, compared to chemotherapy "CPt + TAX". Indeed, a TGI around 25 % at day 26 was obtained with "FD P53-S-LNCs" and "HD P53-S-LNCs" compared to NaCl 0.9 % "control" whereas a significant TGI of 46 % at day 26 was obtained with chemotherapy "CPt + TAX" compared to "control" (**Figure 3.c and Table 4**). Interestingly, the combination of stealth P53-LNCs with chemotherapy "FD P53-S-LNCs + CPt + TAX" improved the efficacy with a significant TGI of 61.9 % compared to NaCl 0.9 % "control". Contrary to the Low OXPHOS model OV54, the observed improvement could be due to the encapsulated P53 itself. Indeed, a TGI of 37.8 % was obtained after treatment by the combination of the stealth blank LNCs and chemotherapy "S-B-LNCs + CPt + TAX", whereas a TGI of 46 % was obtained after the chemotherapy itself "CPt + TAX". Moreover, the obtained results showed a good tendency to improve the anticancer

effect of chemotherapy when associated with stealth P53-LNCs “FD P53-S-LNCs + CPt + TAX” with a decrease of 29 % on the RTV compared to chemotherapy “CPt + TAX” (**Figure 3.d and Table 4**). Another way to express the efficacy of the different treatments consists in using the probability of regression curves. These curves are drawn as theoretical survival curves, where the death of a mouse corresponds to the time to reach the doubling of tumour volume (RTV = 2). The results showed a slight, but not significant, improvement in the time to reach RTV = 2 with the combination of the stealth P53-LNCs and chemotherapy “FD P53-S-LNCs + CPt + TAX” (**Figure 4.b**) compared to chemotherapy “CPt + TAX”, with a median survival of 9.25 days and 8.75 days respectively.

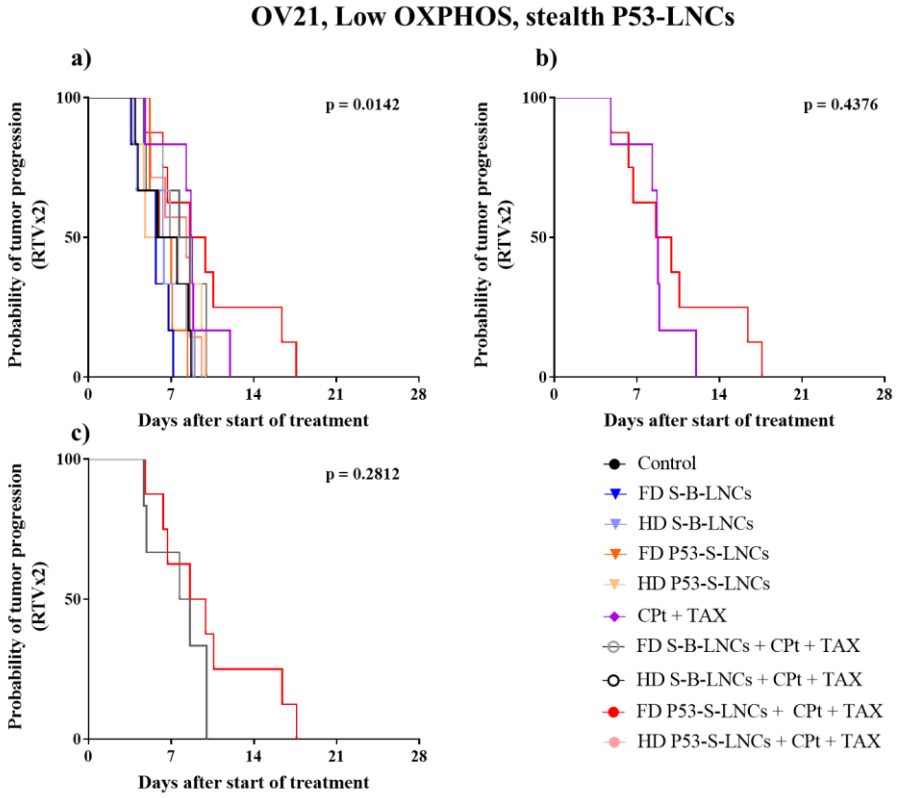


**Figure 4.** a) Probability of tumour progression to reach the doubling of tumour volume (RTVx2) (Kaplan-Meier curves) on Low OXPHOS model OV21 after different treatments, summarized in **Table 3** ; b) Comparison of the Kaplan Meier curves obtained on the Low OXPHOS model OV21 with chemotherapy “CPt + TAX” (purple line) and the combination stealth P53-LNCs and chemotherapy “FD P53-S-LNCs + CPt + TAX”’ (red line); c) Comparison of the Kaplan Meier curves obtained on the Low OXPHOS model OV21 with the combination stealth blank LNCs and chemotherapy “FD S-B-LNCs + CPt + TAX” (grey line) and the combination stealth P53-LNCs and chemotherapy “FD P53-S-LNCs + CPt + TAX” (red line). Statistical analysis was performed with the Log-rank (Mantel-Cox) test. Data were considered significant for $p < 0.05$.

To finish, combining results from the two Low OXPHOS models allowed to express the Overall Response Rate. The combination of stealth P53-LNCs and chemotherapy “FD P53-S-LNCs + CPt + TAX” improved significantly the quality of response compared to chemotherapy “CPt + TAX, with an ORR lower than -0.5 for 69 % and 18 % of treated mice respectively ($p = 0.0218$) (**Figure 5**). However, it was difficult to conclude about the benefit of P53 as 67 % of treated mice with combination of stealth blank LNCs and chemotherapy “FD S-B-LNCs + CPt + TAX” also showed an ORR lower than -0.5 ($p = 0.9787$).

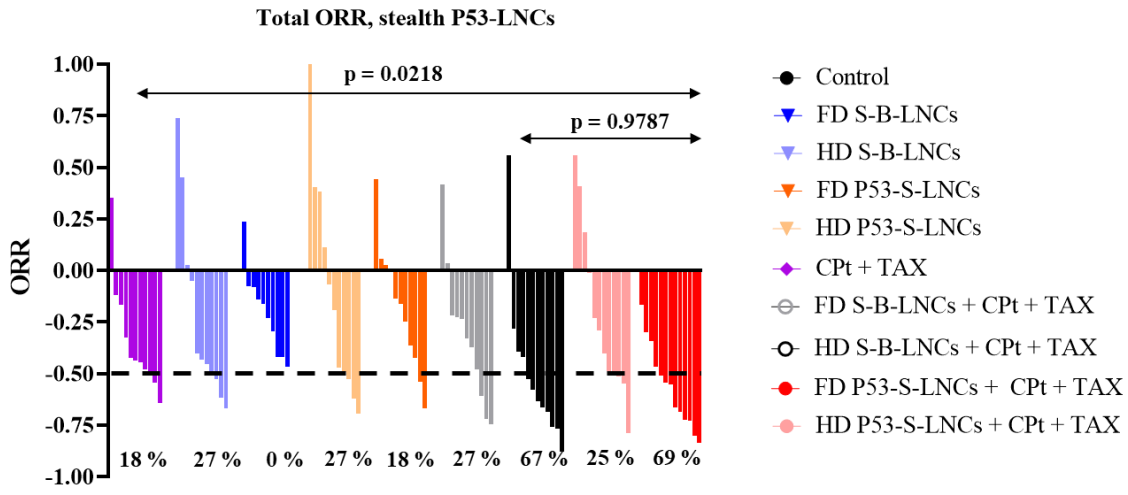


**Figure 5.** Overall Response Rate (ORR) of mice from the two Low OXPHOS models, OV21 and OV54, treated with or without P53. Treatments are summarized in **Table 3.**. The ORR was defined as the relative tumour volume variation (RTVV) of each treated mouse calculated from the following formula *[(Vt/Vc)-1]*, where *Vt* is the volume of the treated mouse and *Vc* the median volume of the corresponding control group at a time corresponding to the end of treatment.

### *3.4. In vivo activity of stealth P722-LNCs on the selected PDX models*

**Table 5**: Summary of the different groups after treatment by stealth P722-LNCs at 0.56 % (w/w) alone or in combination with conventional chemotherapy (carboplatin and paclitaxel). Carboplatin and paclitaxel were intraperitoneally injected once every three weeks at half dose HD (33 mg/kg and 15 mg/kg respectively). Stealth blank and stealth P722-LNCs were intravenously administered twice per week at a dose of 8 mg/kg.

| Treatment | Composition | Dose of anticancer drug (mg/kg) |
|---|---|---|
| **Control** | Control (NaCl 0.9 %) | |
| **S-B-LNCs** | Stealth blank LNCs | eq. 8* |
| **P722-S-LNCs** | Stealth P722-LNCs | 8 |
| **CPt + TAX** | Half dose, carboplatin + paclitaxel | 33 + 15 |
| **S-B-LNCs + CPt + TAX** | Stealth blank LNCs + carboplatin + paclitaxel | eq. 8 + 33 + 15 |
| **P722-S-LNCs + CPt + TAX** | Stealth P722-LNCs + carboplatin + paclitaxel | 8 + 33 + 15 |

eq. 8* indicates that the same concentration in excipients than the full dose stealth P722-LNCs was administered

The antitumour activity of stealth P722-LNCs was assessed *in vivo* on two Low OXPHOS PDX models (OV21 and OV54). The formulation was administered intravenously twice a week, alone or followed by treatment by carboplatin and paclitaxel (once every three weeks). First, tolerance studies were performed, and the results obtained did not show any significant weight loss in the treated groups, indicating again a good tolerance by the mice of the different treatments (**Figure S4.b** in supplementary information).

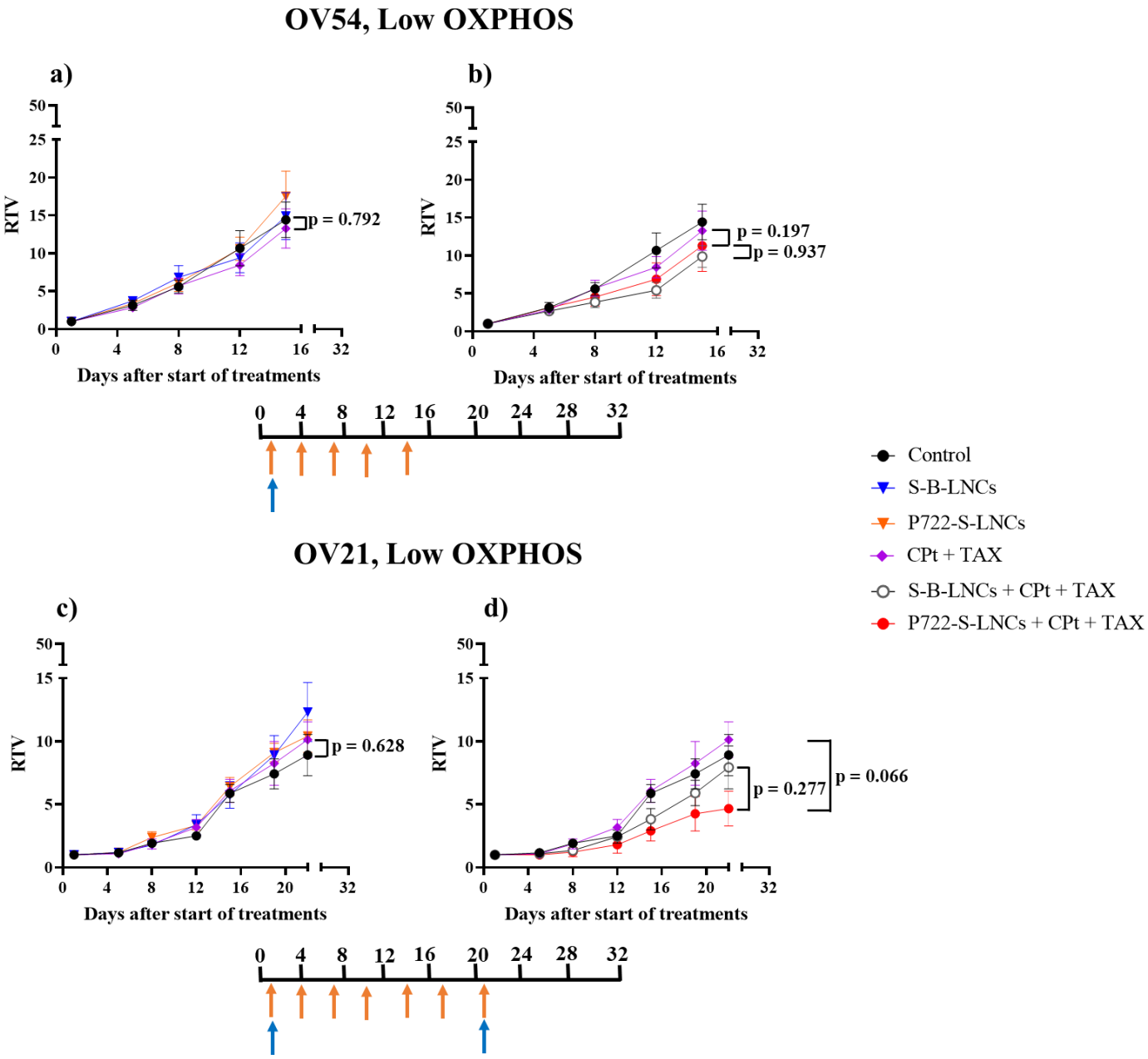


**Figure 6.** a) Comparison of the RTV as a function of time of the Low OXPHOS model OV54 treated with stealth blank LNCs "S-B-LNCs" (blue triangle), stealth P722-LNCs "P722-S-LNCs" (orange triangle) and chemotherapy "CPt + TAX" (purple diamond) ; b) Comparison of the RTV as a function of time of the Low OXPHOS model OV54 treated with combination of stealth blank LNCs and chemotherapy "S-B-LNCs + CPt + TAX" (empty grey circle), stealth P722-LNCs and chemotherapy "P722-S-LNCs + CPt + TAX" (red circle) and chemotherapy "CPt + TAX" (purple diamond) ; c) Comparison of the RTV as a function of time of the Low OXPHOS model OV21 treated with stealth blank LNCs "S-B-LNCs" (blue triangle), stealth P722-LNCs "P722-S-LNCs" (orange triangle) and chemotherapy "CPt + TAX" (purple diamond) ; d) Comparison of the RTV as a function of time of the Low OXPHOS model OV21 treated with combination of stealth blank LNCs and chemotherapy "S-B-LNCs + CPt + TAX" (empty grey circle), stealth P722-LNCs and chemotherapy "P722-S-LNCs + CPt + TAX" (red circle) and chemotherapy "CPt + TAX" (purple diamond). Timelines indicated days of treatment injection for P53-LNCs or blank LNCs (orange arrow) and for chemotherapies (blue arrow). Data are means ± SEM ($5 \leq n \leq 7$ mice per group). Statistical analysis was performed with a Mann-Whitney test to compare two groups each other. Data are considered significant for $p < 0.05$.

**Table 6:** Relative tumour volume ([RTV] = $V_n/V_0$, n corresponding to the end of experiment) and tumour growth inhibition ([TGI] = 100 − (RTVt/ RTVc ×100)) after different treatments, summarized in Table 3, on the two Low OXPHOS model OV21 and OV54.

| | **Treatments** | **RTV (%) (day 15)** | **TGI (%) (day 15)** |
|---|---|---|---|
| **0V54** | Control | 14.4 | 0.0 |
| | S-B-LNCs | 14.9 | -3.4 |
| | P722-S-LNCs | 17.5 | -21.6 |
| | CPt + TAX | 13.3 | 8.0 |
| | S-B-LNCs + CPt + TAX | 9.9 | 31.5 |
| | P722-S-LNCs + CPt + TAX | 11.3 | 21.7 |
| | | **RTV (%) (day 22)** | **RTV (%) (day 22)** |
| **OV21** | Control | 8.9 | 0.0 |
| | S-B-LNCs | 12.3 | -38.4 |
| | P722-S-LNCs | 10.4 | -16.9 |
| | CPt + TAX | 10.1 | -13.7 |
| | S-B-LNCs + CPt + TAX | 7.9 | 11.0 |
| | P722-S-LNCs + CPt + TAX | 4.7 | 47.7 |

RTV evolution on the two Low OXPHOS model, OV21 and OV54, is shown in **Figure 6**. On the Low OXPHOS model OV54 (**Figure 6.a and 6.b and Table 6**), the stealth P722-LNCs "P722-S-LNCs" and chemotherapy "CPt + TAX" did not impact the tumour growth compared to NaCl 0.9 % "control". When combining stealth P722-LNCs with carboplatin and paclitaxel "P722-S-LNCs + CPy + TAX", a TGI of 21.7 % was obtained but again, it was not possible to conclude that this efficacy was due to P722 as a TGI of 31.5 % was obtained after treatment by the combination of stealth blank LNCs and chemotherapy "S-B-LNCs + CPt + TAX". On this model, no antitumour effect was obtained whatever the treatment.

On the Low OXPHOS model OV21, no antitumour activity was induced by chemotherapy, stealth blank LNCs and stealth P722-LNCs ("CPt + TAX", "S-B-LNCs" and "P722-S-LNCs" respectively, **Table 6**). In contrast, the combination of chemotherapy and stealth P722-LNCs "P722-S-LNCs + CPt + TAX" showed a tumour growth inhibition of 54 % on the tumour volume compared to carboplatin and paclitaxel alone "CPt + TAX", similar to what obtained with the combination of stealth P53-LNCs and chemotherapy (46 %, "FD P53-S-LNCs + CPt + TAX", **Table 4**). This represents a real improvement given that the dose in P722 was eight times smaller than the concentration in P53 (8 mg/kg versus 65 mg/kg). Moreover, one mouse showed a complete remission after the combination of chemotherapy and stealth P722-LNCs and another one presented a large decrease of its tumour volume until 70 days (RTV < 0.2), as shown in **Figure 7.a**. Finally, tumoral evolution probability curves showed that the time to reach RTV2 increased significantly when mice were treated with the combination of chemotherapy and stealth P722-LNCs "P722-S-LNCs + CPt + TAX" compared to chemotherapy alone "CPt + TAX" ($p = 0.0322$), with a median survival of 12.2 days and 9.55 days respectively (**Figure 7.b**). Even if the results were not significant ($p = 0.1849$) between combination of stealth blank LNCs and chemotherapy "S-B-LNCs + CPt + TAX" and combination of stealth P722 and chemotherapy "P722-S-LNCs + CPt + TAX" (median survival of 10.65) (**Figure 7.c** and **Table 4**), a clear trend could be seen, indicating that the efficacy observed could be due to the ferrocifen P722 itself. Finally, it was also an improvement compared to the median survival of 9.25 days obtained with the combination of stealth P53-LNCs and chemotherapy "FD P53-S-LNCs + CPt + TAX" (**Table 3**).

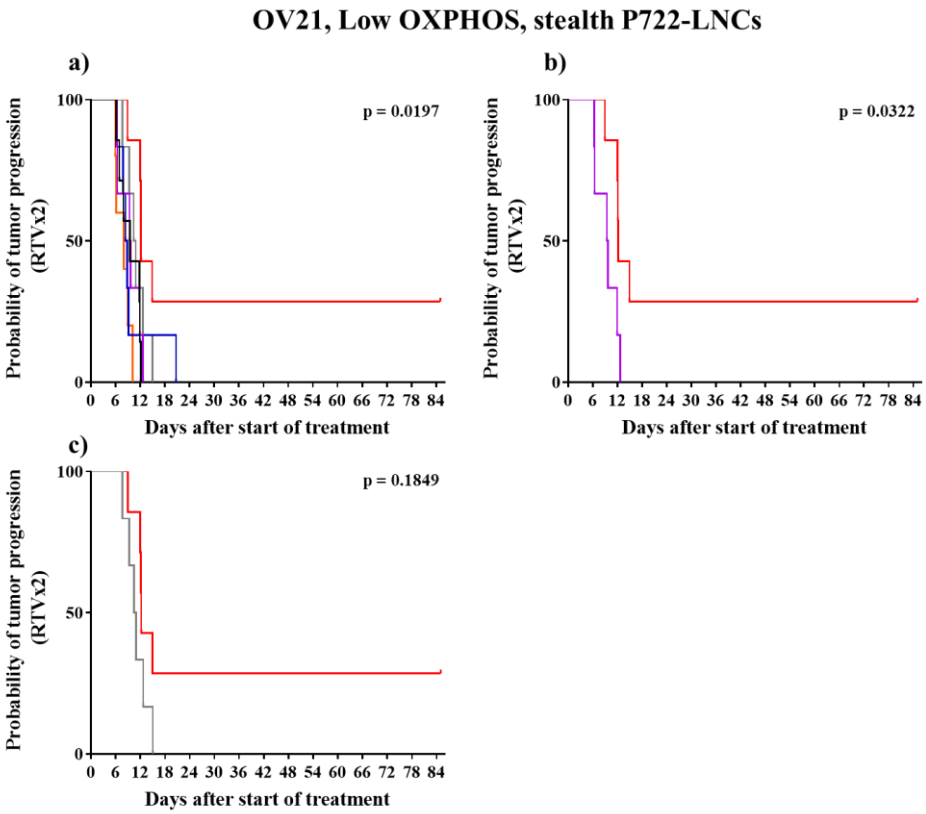


**Figure 7.** a) Probability of tumour progression to reach the doubling of tumour volume (RTVx2) (Kaplan-Meier curves) on Low OXPHOS model OV21 after different treatments, summarized in **Table 5** ; b) Comparison of the Kaplan Meier curves obtained on the Low OXPHOS model OV21 with chemotherapy "CPt + TAX" (purple line) and combination of stealth P722-LNCs and chemotherapy "P722-S-LNCs + CPt + TAX" (red line) ; c) Comparison of the Kaplan Meier curves obtained on the Low OXPHOS model OV21 with combination of stealth blank LNCs and chemotherapy "S-B-LNCs + CPt + TAX" (grey line) and combination of stealth P722-LNCs and chemotherapy "P722-S-LNCs + CPt + TAX" (red line). Statistical analysis was performed with the Log-rank (Mantel-Cox) test. Data were considered significant for $p < 0.05$.

Next, combining results from the two Low OXPHOS models allowed to express the Overall Response Rate. The combination of stealth P722-LNCs and chemotherapy "P722-S-LNCs + CPt + TAX" improved significantly the quality of response compared to chemotherapy "CPt + TAX", with an ORR lower than -0.5 for 54 % and 8 % of treated mice respectively ($p = 0.0472$) (**Figure 8**). For the combination of stealth blank LNCs and chemotherapy "S-B-LNCs + CPt + TAX", 33 % of mice responders were obtained. Even if the percentage of mice responders was lower for combination of stealth P722-LNCs and chemotherapy "P722-S-LNCs + CPt + TAX" (54 %) compared to combination of stealth P53-LNCs and chemotherapy "FD P53-S-LNCs + CPt + TAX" (69 %), it was possible to conclude about the benefit of P722, as the concentration was eight time smaller than for P53 formulations. One complete remission was even obtained with "P722-S-LNC+CPt+TAX" treatment.

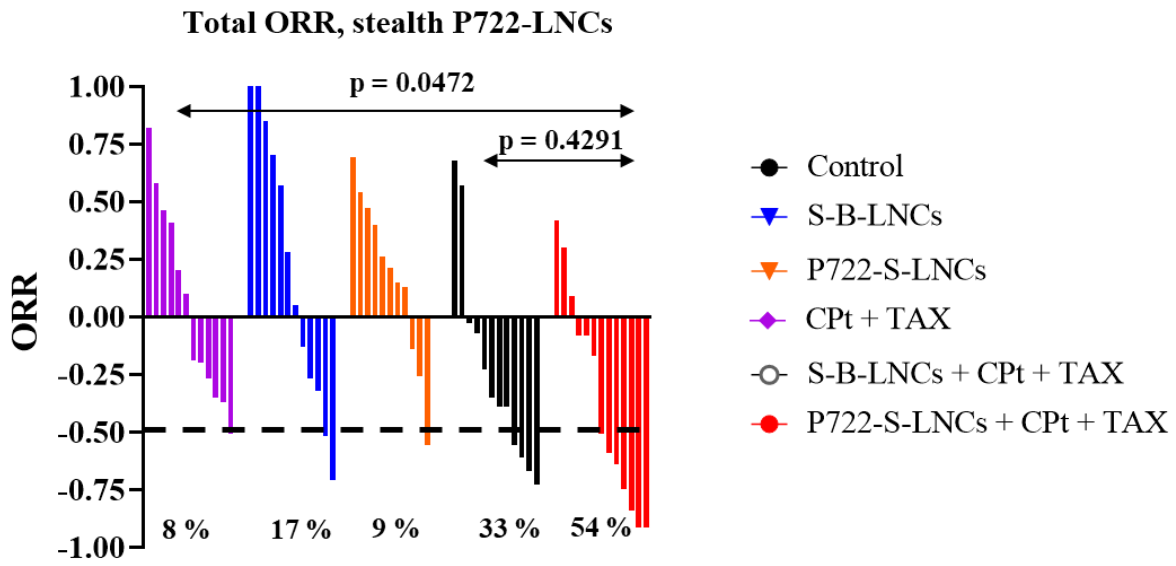


**Figure 5.** Overall Response Rate (ORR) of mice from the two Low OXPHOS models, OV21 and OV54, treated with or without P722. Treatments are summarized in **Table 4.**. The ORR was defined as the relative tumour volume variation (RTVV) of each treated mouse calculated from the following formula *[(Vt/Vc)-1]*, where *Vt* is the volume of the treated mouse and *Vc* the median volume of the corresponding control group at a time corresponding to the end of treatment.

Improvement in the antitumour activity of the treatment combining chemotherapy and stealth P722-LNCs ("P722-S-LNCs + CPt +TAX", **Table 6**), compared to the treatment combining chemotherapy and stealth P53-LNCs ("FD P53-S-LNCs + CPt + TAX", **Table 4**) could be explained by the $IC_{50}$ values, often lower in various cell lines for the P722 than for the P53: for example, on the ovarian cancer SKOV3 and A2780 cell lines or the breast cancer MDA-MB-231 cell line **(15)**. This better efficiency *in vitro* and *in vivo* might be due to the greater stability of the quinone methide (QM) obtained from P722 compared to the one obtained from P53. Indeed, P722-QM had a half-life in acetone of about 10 days compared to 30 h for P53-QM, due to a surprising intramolecular lone-pair-π interaction between the oxygen of the succimido ring and the phenol in the trans position **(33)**. This extra stabilizing lone pair-π interaction is unprecedented and possibly provides an explanation for the exceptional cytotoxicity of P722, with $IC_{50}$ in the nanomolar range. Therefore, it is thought that P722-QM could more easily react with biological targets such as thioredoxin reductase (TrxR) and glutathione compared to other ferrocifens already tested **(36–38)**. Indeed, its electrophilicity would allow it to react with the nucleophilic selenocysteine located in the active site of thioredoxin reductase TrxR via a Michael addition. TrxR, an enzyme of the Trx system involved in redox regulation, is often expressed in cancer cells. Inhibition of the TrxR could counteract the ability of the tumour cell to defend itself against oxidative stress **(39,40)**. Since QM is known as a Michael acceptor, it might be also associated with the reactivation of the tumour suppressor gene TP53, for which mutation is identified in 96 % of ovarian High-Grade-Serous Carcinoma **(41)**. Indeed, it was shown that APR-246, a clinical-stage compound that reactivates the mutant gene TP53, was able to sensibilize a cisplatin-resistant ovarian cancer cell line to cisplatin by inhibiting intracellular free glutathione, a protein known in redox regulation, and to increase chemoresistance to platinum therapy **(42)**. Furthermore, these studies highlighted the role of ROS in ovarian cancer. ROS are essential to initiate the oxidation of Fe(II) to Fe(III) leading to ROS production in a positive feedback loop and so to higher ROS content in tumour cells **(43)**. So, it may be possible, as anticipated, that an increase in oxidative stress occurs due to the action of ferrocifen in the Low OXPHOS model OV21, leading to increased sensitivity to carboplatin and paclitaxel as for the High OXPHOS models **(8)**.

It is not the first time that treatment with ferrocifen LNCs, alone or in combination, have shown better *in vivo* efficiency compared to FDA-approved conventional drugs. Indeed, in 2017, Resnier *et al.* evidenced, on a metastatic melanoma model, higher decrease of the tumour volume after ferrocifen-LNC treatment than for dacarbazine, a chemotherapeutic molecule currently used commercially to treat melanoma **(31)**. Other studies highlighted antitumour effects of different therapies tested on the PDX ovarian cancer model. For example, Bougherara *et al.* showed the potential benefit of targeting anti-Müllerian hormone type II receptor (AMHRII) by combining 3C23K, a humanized monoclonal antibody, with standard chemotherapy **(44)**. Moreover, Harris *et al.* showed that targeting the HER2 tyrosine-protein kinase receptor by using pertuzumab, a humanized monoclonal antibody, improved the response to standard chemotherapy (carboplatin and paclitaxel) **(45)**. In another study, Qi *et al.* reported that nanoparticle-drug conjugates of monomethyl auristatin E (MMAE), a highly potent toxin, improved the tumour growth inhibition compared to cisplatin **(46)**. These studies showed that several strategies could be used to treat ovarian cancer. However, to our knowledge, it is the first time that a treatment with a ROS producer molecule such as ferrocifen potentialized chemotherapy on such advanced preclinical models **(42,47)**, known to be closer to clinical reality **(24)**.

## 4. Conclusion

Ovarian cancer can be classified according to its mitochondrial metabolism, the High OXPHOS ovarian cancer showing a chemosensitivity to standard chemotherapy and the Low OXPHOS ovarian cancer showing a chemoresistant **(8)**. The objective of this work was to evaluate the efficiency *in vivo* of ferrocifen LNCs, alone or in combination with carboplatin and paclitaxel, on advanced PDX ovarian adenocarcinoma models. Two ferrocifens, P53 and P722, known for their high *in vitro* efficiency on several multidrug-resistant cancer cell lines like ovarian cancer, were encapsulated in LNCs. First, the surface modification of LNCs by the PEGylated phospholipids DSPE-$PEG_{2000}$ and the increase of P53 payload in LNCs revealed a potentialization of the combination of stealth P53-LNCs and standard chemotherapy. Then, the use of stealth P722-LNCs in combination with chemotherapy showed a similar therapeutic response (reduction around 50 % of the tumour volume). However, P722 concentration was eight times smaller than P53 (8 mg/kg versus 65 mg/kg) and one mouse was even in complete remission. This dose reduction constitutes an expected improvement which could lead to a decrease in side effects and toxicity. For further studies, it could be interesting to evaluate the potential adjuvant effect of LNCs. Some previous studies highlighted the benefits of using stealth LNCs compared to conventional one. Indeed, Hoarau *et al.* demonstrated a blood half-life of 8 h and 1 h for stealth LNCs and conventional LNCs respectively, with a renal and splenic clearance **(48–50)**. Years later, Lainé *et al.* confirmed that stealth LNCs exhibited a higher circulation time in blood than conventional one, allowing a better accumulation in tumour site, as shown by Morille *et al.* without any hepatic damage **(21,23)**.
Nevertheless, this study confirmed the potential therapeutic interest of ferrocifen stealth LNCs in combination with chemotherapy in PDX models, known to be more representative of the tumour microenvironment of human patients. This is opening the way to potent new organometallic anticancer drug candidates for the treatment of chemoresistant cancers.

**Author contribution**:
**Pierre Idlas**: Formal analysis, Writing - original draft, Writing – review & editing. **Abdallah Ladaycia**: Formal analysis, Writing - original draft, Writing – review & editing. **Fariba Nemati**: Formal analysis, Writing – review & editing. **Elise Lepeltier:** Conceptualization, Methodology, Supervision, Writing – review & editing. **Pascal Pigeon:** Conceptualization, Methodology. **Gérard**

**Jaouen**: Conceptualization, Methodology, Writing – review & editing. **Didier Decaudin**: Conceptualization, Methodology, Supervision, Writing – review & editing. **Catherine Passirani**: Conceptualization, Methodology, Supervision, Writing – review & editing.

**Acknowledgements**

The authors would like to thank the SME Feroscan for its supply of ferrocifens and COST Action STRATAGEM, CA17104. This work was funded by the Agence Nationale de la Recherche (ANR PRCE NaTeMOc N° ANR-19-CE18-0022-01).

**Conflict of interest**

The authors declare no conflict of interest. The authors declare no competing financial interest or personal relationship that could have appeared to influence the work reported in this paper.

**References**

1. Cancer Tomorrow [Internet]. [cited 2022 Apr 21]. Available from: https://gco.iarc.fr/tomorrow/en/dataviz/isotype?types=1&sexes=0&mode=population&group_populations=1&multiple_populations=1&multiple_cancers=0&cancers=25&populations=903_904_905_908_909_935&single_unit=10000

2. Matulonis UA, Sood AK, Fallowfield L, Howitt BE, Sehouli J, Karlan BY. Ovarian cancer. Nat Rev Dis Primers. 2016 Aug 25;2(1):1–22.

3. De Picciotto N, Cacheux W, Roth A, Chappuis PO, Labidi-Galy SI. Ovarian cancer: Status of homologous recombination pathway as a predictor of drug response. Crit Rev Oncol Hematol. 2016 May;101:50–9.

4. Cho KR, Shih IM. Ovarian cancer. Annu Rev Pathol. 2009;4:287–313.

5. da Cunha Colombo Bonadio RR, Fogace RN, Miranda VC, Diz M del PE. Homologous recombination deficiency in ovarian cancer: a review of its epidemiology and management. Clinics (Sao Paulo) [Internet]. 2018 [cited 2020 Apr 8];73(Suppl 1). Available from: https://www.ncbi.nlm.nih.gov/pmc/articles/PMC6096977/

6. Hanahan D. Hallmarks of Cancer: New Dimensions. Cancer Discovery. 2022 Jan 12;12(1):31–46.

7. Gentric G, Mieulet V, Mechta-Grigoriou F. Heterogeneity in Cancer Metabolism: New Concepts in an Old Field. Antioxid Redox Signal. 2017 20;26(9):462–85.

8. Gentric G, Kieffer Y, Mieulet V, Goundiam O, Bonneau C, Nemati F, et al. PML-Regulated Mitochondrial Metabolism Enhances Chemosensitivity in Human Ovarian Cancers. Cell Metab. 2019 08;29(1):156-173.e10.

9. Jaouen G, Top S, Vessières A, Leclercq G, Quivy J, Jin L, et al. The first organometallic antioestrogens and their antiproliferative effects. Comptes Rendus de l'Académie des Sciences - Series IIC - Chemistry. 2000 Apr 1;3(2):89–93.

10. Michard Q, Jaouen G, Vessieres A, Bernard BA. Evaluation of cytotoxic properties of organometallic ferrocifens on melanocytes, primary and metastatic melanoma cell lines. J Inorg Biochem. 2008 Nov;102(11):1980–5.

11. Topin-Ruiz S, Mellinger A, Lepeltier E, Bourreau C, Fouillet J, Riou J, et al. p722 ferrocifen loaded lipid nanocapsules improve survival of murine xenografted-melanoma via a potentiation of apoptosis and an activation of CD8+ T lymphocytes. Int J Pharm. 2021 Jan 25;593:120111.

12. Hillard E, Vessières A, Le Bideau F, Plazuk D, Spera D, Huché M, et al. A series of unconjugated ferrocenyl phenols: prospects as anticancer agents. ChemMedChem. 2006 May;1(5):551–9.

13. Wang Y, Pigeon P, Top S, McGlinchey MJ, Jaouen G. Organometallic Antitumor Compounds: Ferrocifens as Precursors to Quinone Methides. Angew Chem Int Ed Engl. 2015 Aug 24;54(35):10230–3.

14. Wang Y, Dansette PM, Pigeon P, Top S, McGlinchey MJ, Mansuy D, et al. A new generation of ferrociphenols leads to a great diversity of reactive metabolites, and exhibits remarkable antiproliferative properties. Chem Sci. 2018 Jan 7;9(1):70–8.

15. Pigeon P, Wang Y, Top S, Najlaoui F, Garcia Alvarez MC, Bignon J, et al. A New Series of Succinimido-ferrociphenols and Related Heterocyclic Species Induce Strong Antiproliferative Effects, Especially against Ovarian Cancer Cells Resistant to Cisplatin. J Med Chem. 2017 Oct 26;60(20):8358–68.

16. Lollo G, Ullio-Gamboa G, Fuentes E, Matha K, Lautram N, Benoit JP. In vitro anti-cancer activity and pharmacokinetic evaluation of curcumin-loaded lipid nanocapsules. Mater Sci Eng C Mater Biol Appl. 2018 Oct 1;91:859–67.

17. Najlaoui F, Pigeon P, Aroui S, Pezet M, Sancey L, Marrakchi N, et al. Anticancer properties of lipid and poly(ε-caprolactone) nanocapsules loaded with ferrocenyl-tamoxifen derivatives. J Pharm Pharmacol. 2018 Nov;70(11):1474–84.

18. Buriez O, Heldt JM, Labbé E, Vessières A, Jaouen G, Amatore C. Reactivity and Antiproliferative Activity of Ferrocenyl–Tamoxifen Adducts with Cyclodextrins against Hormone-Independent Breast-Cancer Cell Lines. Chemistry – A European Journal. 2008 Sep 19;14(27):8195–203.

19. Idlas P, Lepeltier E, Jaouen G, Passirani C. Ferrocifen Loaded Lipid Nanocapsules: A Promising Anticancer Medication against Multidrug Resistant Tumors. Cancers (Basel). 2021 May 11;13(10):2291.

20. Karim R, Lepeltier E, Esnault L, Pigeon P, Lemaire L, Lépinoux-Chambaud C, et al. Enhanced and preferential internalization of lipid nanocapsules into human glioblastoma cells: effect of a surface-functionalizing NFL peptide. Nanoscale. 2018 Jul 19;10(28):13485–501.

21. Lainé AL, Gravier J, Henry M, Sancey L, Béjaud J, Pancani E, et al. Conventional versus stealth lipid nanoparticles: formulation and in vivo fate prediction through FRET monitoring. J Control Release. 2014 Aug 28;188:1–8.

22. Huynh NT, Morille M, Bejaud J, Legras P, Vessieres A, Jaouen G, et al. Treatment of 9L gliosarcoma in rats by ferrociphenol-loaded lipid nanocapsules based on a passive targeting strategy via the EPR effect. Pharm Res. 2011 Dec;28(12):3189–98.

23. Morille M, Montier T, Legras P, Carmoy N, Brodin P, Pitard B, et al. Long-circulating DNA lipid nanocapsules as new vector for passive tumor targeting. Biomaterials. 2010 Jan;31(2):321–9.

24. Decaudin D. Primary human tumor xenografted models ('tumorgrafts') for good management of patients with cancer. Anticancer Drugs. 2011 Oct;22(9):827–41.

25. Laurent C, Gentien D, Piperno-Neumann S, Némati F, Nicolas A, Tesson B, et al. Patient-derived xenografts recapitulate molecular features of human uveal melanomas. Mol Oncol. 2013 Jun;7(3):625–36.

26. Reyal F, Guyader C, Decraene C, Lucchesi C, Auger N, Assayag F, et al. Molecular profiling of patient-derived breast cancer xenografts. Breast Cancer Res. 2012 Jan 16;14(1):R11.

27. Gao H, Korn JM, Ferretti S, Monahan JE, Wang Y, Singh M, et al. High-throughput screening using patient-derived tumor xenografts to predict clinical trial drug response. Nat Med. 2015 Nov;21(11):1318–25.

28. Izumchenko E, Paz K, Ciznadija D, Sloma I, Katz A, Vasquez-Dunddel D, et al. Patient-derived xenografts effectively capture responses to oncology therapy in a heterogeneous cohort of patients with solid tumors. Ann Oncol. 2017 Oct 1;28(10):2595–605.

29. Pigeon P, Görmen M, Kowalski K, Müller-Bunz H, McGlinchey MJ, Top S, et al. Atypical McMurry Cross-Coupling Reactions Leading to a New Series of Potent Antiproliferative Compounds Bearing the Key [Ferrocenyl-Ene-Phenol] Motif. Molecules. 2014 Jul;19(7):10350–69.

30. Heurtault B, Saulnier P, Pech B, Proust JE, Benoit JP. A novel phase inversion-based process for the preparation of lipid nanocarriers. Pharm Res. 2002 Jun;19(6):875–80.

31. Resnier P, Galopin N, Sibiril Y, Clavreul A, Cayon J, Briganti A, et al. Efficient ferrocifen anticancer drug and Bcl-2 gene therapy using lipid nanocapsules on human melanoma xenograft in mouse. Pharmacol Res. 2017 Dec;126:54–65.

32. Gruosso T, Garnier C, Abelanet S, Kieffer Y, Lemesre V, Bellanger D, et al. MAP3K8/TPL-2/COT is a potential predictive marker for MEK inhibitor treatment in high-grade serous ovarian carcinomas. Nat Commun. 2015 Oct 12;6:8583.

33. Wang Y, Pigeon P, Top S, Sanz García J, Troufflard C, Ciofini I, et al. Atypical Lone Pair-π Interaction with Quinone Methides in a Series of Imido-Ferrociphenol Anticancer Drug Candidates. Angew Chem Int Ed Engl. 2019 17;58(25):8421–5.

34. Vonarbourg A, Passirani C, Saulnier P, Benoit JP. Parameters influencing the stealthiness of colloidal drug delivery systems. Biomaterials. 2006 Aug;27(24):4356–73.

35. Huynh NT, Passirani C, Allard-Vannier E, Lemaire L, Roux J, Garcion E, et al. Administration-dependent efficacy of ferrociphenol lipid nanocapsules for the treatment of intracranial 9L rat gliosarcoma. Int J Pharm. 2012 Feb 14;423(1):55–62.

36. Wang Y, Richard MA, Top S, Dansette PM, Pigeon P, Vessières A, et al. Ferrocenyl Quinone Methide-Thiol Adducts as New Antiproliferative Agents: Synthesis, Metabolic Formation from Ferrociphenols, and Oxidative Transformation. Angew Chem Int Ed Engl. 2016 22;55(35):10431–4.

37. Citta A, Folda A, Bindoli A, Pigeon P, Top S, Vessières A, et al. Evidence for Targeting Thioredoxin Reductases with Ferrocenyl Quinone Methides. A Possible Molecular Basis for the Antiproliferative Effect of Hydroxyferrocifens on Cancer Cells. J Med Chem. 2014 Nov 13;57(21):8849–59.

38. Scalcon V, Citta A, Folda A, Bindoli A, Salmain M, Ciofini I, et al. Enzymatic oxidation of ansa-ferrocifen leads to strong and selective thioredoxin reductase inhibition in vitro. J Inorg Biochem. 2016;165:146–51.

39. Arnér ESJ, Holmgren A. The thioredoxin system in cancer. Seminars in Cancer Biology. 2006 Dec 1;16(6):420–6.

40. Arnér ESJ. Targeting the Selenoprotein Thioredoxin Reductase 1 for Anticancer Therapy. Adv Cancer Res. 2017;136:139–51.

41. Cole AJ, Dwight T, Gill AJ, Dickson KA, Zhu Y, Clarkson A, et al. Assessing mutant p53 in primary high-grade serous ovarian cancer using immunohistochemistry and massively parallel sequencing. Sci Rep. 2016 May 18;6(1):26191.

42. Mohell N, Alfredsson J, Fransson Å, Uustalu M, Byström S, Gullbo J, et al. APR-246 overcomes resistance to cisplatin and doxorubicin in ovarian cancer cells. Cell Death Dis. 2015 Jun;6(6):e1794–e1794.

43. Jaouen G, Vessières A, Top S. Ferrocifen type anti cancer drugs. Chem Soc Rev. 2015 Dec 21;44(24):8802–17.

44. Bougherara H, Némati F, Nicolas A, Massonnet G, Pugnière M, Ngô C, et al. The humanized anti-human AMHRII mAb 3C23K exerts an anti-tumor activity against human ovarian cancer through tumor-associated macrophages. Oncotarget. 2017 Nov 21;8(59):99950–65.

45. Harris FR, Zhang P, Yang L, Hou X, Leventakos K, Weroha SJ, et al. Targeting HER2 in patient-derived xenograft ovarian cancer models sensitizes tumors to chemotherapy. Mol Oncol. 2019 Feb;13(2):132–52.

46. Qi R, Wang Y, Bruno PM, Xiao H, Yu Y, Li T, et al. Nanoparticle conjugates of a highly potent toxin enhance safety and circumvent platinum resistance in ovarian cancer. Nat Commun. 2017 Dec 18;8(1):2166.

47. Yang X, Lyer AK, Singh A, Choy E, Hornicek FJ, Amiji MM, et al. MDR1 siRNA loaded hyaluronic acid-based CD44 targeted nanoparticle systems circumvent paclitaxel resistance in ovarian cancer. Sci Rep. 2015 Feb 17;5(1):8509.

48. Hoarau D, Delmas P, David S, Roux E, Leroux JC. Novel long-circulating lipid nanocapsules. Pharm Res. 2004 Oct;21(10):1783–9.

49. Lacoeuille F, Hindre F, Moal F, Roux J, Passirani C, Couturier O, et al. In vivo evaluation of lipid nanocapsules as a promising colloidal carrier for paclitaxel. Int J Pharm. 2007 Nov 1;344(1–2):143–9.

50. Ballot S, Noiret N, Hindré F, Denizot B, Garin E, Rajerison H, et al. 99mTc/188Re-labelled lipid nanocapsules as promising radiotracers for imaging and therapy: formulation and biodistribution. Eur J Nucl Med Mol Imaging. 2006 May;33(5):602–7.